Published by Avanti Publishers

Journal of Advanced Thermal Science Research

ISSN (online): 2409-5826

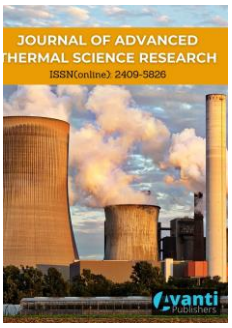

Comparative Study on Interphase Force Model of Gas-Liquid Two-Phase Bubbly Flow Based on OpenFOAM

Chang Liu[1], Haochuang Wu[2,*], Wei Lu[3], Deqi Chen[1], Junjie Pan[3], Zhenzhong Li[1] and Jintao Feng[3]

[1]*Key Laboratory of Low-grade Energy Utilization Technologies and Systems (Chongqing University), Ministry of Education, Chongqing, 400044, China*

[2]*College of Primary Education, Chongqing Normal University, Chongqing, 400030, China*

[3]*Key Laboratory of Nuclear Reactor System Design Technology, China Nuclear Power Research and Design Institute, Chengdu, 610041, China*

ARTICLE INFO

Article Type: Research Article

Keywords:
DEDALE
Bubbly flow
OpenFOAM
Two-fluid model
Interphase force model

Timeline:
Received: January 03, 2022
Accepted: April 05, 2022
Published: June 07, 2022

Citation: Liu C, Wu H, Lu W, Chen D, Pan J, Li Z, Feng J. Comparative Study on Interphase Force Model of Gas-Liquid Two-Phase Bubbly Flow Based on OpenFOAM. J Adv Therm Sci Res. 2022; 9: 24-37.

DOI: https://doi.org/10.15377/2409-5826.2022.09.3

ABSTRACT

It is essential to choose an appropriate interphase force model when studying gas-liquid two-phase bubbly flow by numerical calculation. Because of the complexity of gas-liquid interaction, researchers have developed many models, while there is still a lack of corresponding guidelines when selecting the combination of interphase force models. In the present study, taking the DEDALE experimental condition as the research object, the parameter distribution characteristics of void fraction and gas-liquid two-phase velocity under the experimental condition are simulated, and the calculation results of different interphase force models are analyzed and compared with the experimental results. The effects of different interphase force models on the local parameter distribution characteristics of the two phases are analyzed and discussed, and the optimal model combination under this experimental condition is obtained.

*Corresponding Author
Email: hch_wu@cqnu.edu.cn
Tel: 86-23-65102052

1. Introduction

The phenomenon of gas-liquid two-phase flow exists widely in energy and power engineering, especially in nuclear reactors, where bubbly flow directly affects the safety and performance of nuclear reactors. In the two-phase flow system, the void fraction distribution is an important parameter for predicting a two-phase flow pattern, and the prediction of local parameter distribution plays an important role in estimating the running state of the system. As an analytical model which can accurately describe the two-phase flow, the two-fluid model gives the respective conservation equations of the two-phase fluid. In the gas-liquid two-phase flow, the two phases are not independent, and there is an interphase transfer of mass, momentum, and energy. These transfer terms are completed through the interphase interface, the key of the two-fluid model. Usually, the interfacial transfer terms can be formulated as the product of the interfacial area concentration (IAC) and the driving term (e.g., temperature gradient, velocity gradient). The interfacial area concentration is defined as the interfacial area per unit volume, which quantifies the area for the interfacial transfer process. For adiabatic bubbly flow, momentum transfer is the only interface transfer mechanism, which can be characterized by interphase forces, including drag force, lift force, wall lubrication force, turbulent dispersion force, and virtual mass force. At present, researchers have developed many models for different interphase forces. The local parameters of the two phases result from the comprehensive action of all the interphase forces, and it is a challenge to evaluate the model independently of each other. Therefore, the researchers discussed the different model combinations of adiabatic bubbly flow.

Based on the Tomiyama [1] drag model, Lucas *et al*. [2] numerically simulated the vertical polydisperse air-water flow experiments MTLoop [3] and TOPFLOW [4] to evaluate the combination of different transverse interphase force models. It is found that the combination of the Tomiyama lift model, Tomiyama wall lubrication force model, and Favre average drag (FAD) [5] turbulent dispersion force model has the best prediction effect in the range of superficial liquid velocity $j_l \leq 1.0\mathrm{m/s}$ and superficial gas velocity $j_g \leq 0.53\mathrm{m/s}$. Yamoah *et al*. [6] used different interphase force models to simulate the air-water bubbly flow experiments of Monrósandreu *et al*. [7]. It is found that the prediction results are closest to the experimental data by using the combination of the Grace [8] drag model, Tomiyama lift model, Antal [9] wall lubrication force model, and FAD turbulent dispersion force model. Wang and Yao [10] analyzed the applicable scope of the interphase force model, verified the model based on three bubbly flow experiments carried out by Hibiki *et al*. [3,11,12], and proposed the best model combination of different Re_b ranges: Grace, Tomiyama and Ishii-Zuber [13] drag model, Hosokawa [14] wall lubrication force model, FAD turbulent dispersion force model suitable for the whole Re_b range. Saffman-Mei [15,16] lift model is suitable for low Re_b flow, while Tomiyama lift model has better simulation accuracy for medium Re_b flow. In addition, Tomiyama and Moraga [17] lift model have the best simulation effect for high Re_b flow. Liao *et al.* [18] proposed a closed model of adiabatic bubbly flow, which was verified by gas-liquid two-phase flow in vertical tubes and bubble column experiments. The results show that the simulation effect of the model is good under various conditions. Table **1** is a partial summary of the verification of the interphase force model of vertical upward bubbly flow.

Table 1: Comparative analysis of interphase force models in the vertical upward flow.

Researchers	Drag Force	Lift Force	Wall Lubrication Force	Turbulent Dispersion Force	Parameter Range
Lucas *et al*. [2]	Tomiyama	Tomiyama	Tomiyama	FAD	j_l≤1.0m/s j_g≤0.53m/s
Yamoah *et al*. [6]	Grace	Tomiyama	Antal	FAD	j_l≤1.0m/s j_g≤0.3m/s
Wang and Yao [10]	Grace/ Tomiyama/ Ishii-Zuber	Saffman-Mei Tomiyama Tomiyama/ Moraga	Hosokawa	FAD	j_l=0.491m/s j_g=0.0556m/s j_l=0.405m/s j_g=0.0111m/s j_l=2.607m/s j_g=1.275m/s
Liao *et al*. [18]	Ishii-Zuber	Tomiyama	Hosokawa	FAD	j_l≤1.067m/s j_g≤1.045m/s

So far, no consensus has been reached on the combination of the interphase force model. This situation greatly limits the ability of computational fluid dynamics to predict the bubbly flow. In the present study, taking the DEDALE experiment carried out by EDF [19] as the research object, the vertical bubbly flow is simulated, and different interphase force models are analyzed and compared. Different model combinations are selected to simulate the vertical circular tube, and their effects on local parameters such as void fraction, gas velocity, and liquid velocity distribution are obtained. The maximum error and root mean square error between the numerical results of each model combination and the experimental values are calculated, and a set of reasonable model combinations to simulate the experimental condition is obtained.

2. Mathematical Model

2.1. Two-Fluid Model

The governing equations of the two-fluid model can be averagely obtained from the basic equations of each phase, and both the continuous phase and the discrete phase are treated as continuous phases under the Euler coordinate system, and the mass and momentum conservation equations of each phase are established respectively. The momentum transfer between the phases is characterized by the momentum transfer term in the equation. The continuity equations of the gas phase and liquid phase can be written as follows:

$$\frac{\partial(\alpha_k\rho_k)}{\partial t}+\nabla\cdot(\alpha_k\rho_k\overline{U}_k)=0 \tag{1}$$

where *k* represents liquid phase or gas phase, α , ρ_k and $\overline{U}_k$ denote phase fraction, density, and averaged velocity, respectively.

The two-phase momentum equation is expressed as follows:

$$\frac{\partial(\alpha_k\rho_k\overline{U}_k)}{\partial t}+\nabla\cdot(\alpha_k\rho_k\overline{U}_k\overline{U}_k)=-\alpha_k\nabla p+\nabla\cdot[\alpha_k(\nabla\overline{U}_k+(\nabla\overline{U}_k)^T)]+\alpha_k\rho_k\vec{g}+\vec{F}_k \tag{2}$$

where μ_k^{eff} is effective viscosity which is the sum of the molecular and the turbulent viscosities, the definition will be introduced in the next section, and $\vec{F}_k$ is the total interphase force, which will be explained in detail below.

2.2. Two-Phase Turbulence Model

Because the two-fluid model is more complex than the single-fluid model and its development is not mature enough, the closed equations in the model are mostly empirical or semi-empirical formulas. In the process of simulation calculation, the corresponding closed equations should be constructed and selected according to specific problems. The accuracy of *k-ε* model has been greatly verified in engineering applications. In this paper, it is used as a turbulence model, and its expression is as follows:

$$\frac{\partial(\alpha_i\rho_ik_i)}{\partial t}+\nabla\cdot\left(\alpha_i(\rho_i\overline{U}_ik_i-(\mu_i+\frac{\mu_i^T}{\sigma_k})\nabla k_i)\right)=\alpha_iS_{i,k}+(\dot{m}_{ij}k_j-\dot{m}_{ji}k_i) \tag{3}$$

$$\frac{\partial(\alpha_i\rho_i\varepsilon_i)}{\partial t}+\nabla\cdot\left(\alpha_i(\rho_i\overline{U}_i\varepsilon_i-(\mu_i+\frac{\mu_i^T}{\sigma_\varepsilon})\nabla\varepsilon_i)\right)=\alpha_iS_{i,\varepsilon}+(\dot{m}_{ij}\varepsilon_j-\dot{m}_{ji}\varepsilon_i) \tag{4}$$

where *i* represents liquid phase or gas phase, k, ε, μ, μ^T, S and $\dot{m}_{ij}$ denote turbulent kinetic energy, turbulent energy dissipation rate, viscosity, turbulent viscosity, source phase, and mass transfer rate from *j* phase to *i* phase, respectively.

Due to the large density difference between gas and liquid, it is considered that the bubble fluctuates with the liquid turbulence. Assuming that the gas phase is laminar flow, it only affects the turbulent kinetic energy *k* and turbulent dissipation rate of the liquid phase *ε*. This paper introduces the Sato model (considering the additional influence of discrete relative continuous phase and bubble-induced turbulence). In the simulation process, the

turbulent viscosity of the liquid phase is defined as the linear sum of turbulent viscosity caused by shear and turbulent viscosity caused by bubble, as follows:

$$\mu^T = \rho_l C_\mu \frac{k_l^2}{\epsilon_l} + C_{\mu b} d_b \alpha_v |\overline{U}_v - \overline{U}_l| \tag{5}$$

The first term on the right side of the equation is the turbulent viscosity caused by shear, and the second term is the turbulent viscosity caused by bubbles, $C_\mu = 0.09$, $C_{\mu b} = 0.6$. Therefore, the effective turbulent viscosity of the liquid phase and gas phase is respectively:

$$\mu_l^{eff} = \mu_l + \mu_l^T = \mu_l + \rho_l C_\mu \frac{k_l^2}{\epsilon_l} + \frac{1}{2} C_{\mu b} \rho_l d_b \alpha_v |\overline{U}_v - \overline{U}_l| \tag{6}$$

$$\mu_v^{eff} = \mu_v \tag{7}$$

2.3. Models for Interfacial Forces

When the two-fluid model is used to simulate the flow field, the interphase force term in the momentum conservation equation needs to be closed by the interphase force model. The momentum exchange between phases is the momentum transfer between phases per unit volume at the phase interface. The momentum exchange between phases is calculated by solving the momentum equations of the liquid phase and gas phase. The interfacial momentum force is usually added as a source term in the momentum equation. In general, there is relative motion between the two phases, and the bubbles in the flowing liquid are always affected by the interphase forces, which are caused by the inhomogeneous distribution of drag and stress on the bubble surface. The interfacial term is the sum of the mean part, including drag force, lift force, virtual added mass force, wall lubrication force, and a turbulent part commonly modeled proportionally to the void fraction gradient.

In using the two-fluid model to simulate the two-phase flow, there is a key problem: what form of interphase force model is used to describe the interphase interaction, which is also the main research content of this paper.

2.3.1. Drag Force

Drag force is the most important force of momentum transfer between gas and liquid, which characterizes the blocking effect of surrounding liquid on moving bubbles. In terms of unit volume, the following relations are used to calculate the drag force:

$$\vec{F}_g^{\,D} = -\frac{3}{4}\frac{C_D}{d_b}\alpha_g \rho_l \left\|\vec{U}_g - \vec{U}_l\right\|\left(\vec{U}_g - \vec{U}_l\right) \tag{8}$$

where C_D is the drag coefficient. It can be calculated by different mathematical expressions, as shown in Table **2**.

2.3.2. Lift Force

During the bubble motion, due to the asymmetry of the liquid phase flowing on both sides of its movement direction, the pressure on both sides of the bubble will be unbalanced, resulting in lift perpendicular to the direction of the bubble movement. After being subjected to liquid phase shear flow, drag force, and vortex, the large bubble is prone to deformation, and a deflected tail vortex is generated behind the bubble, which promotes the lateral movement of the bubble. In bubbly flow, the lift per unit volume is defined by the following equation:

$$\vec{F}_g^{\,L} = -C_L \rho_l \alpha_g \left(\vec{U}_g - \vec{U}_l\right) \times \left(\nabla \times \vec{U}_l\right) \tag{9}$$

Where C_L is the lift coefficient which is very important to the bubble's motion. If the sign of bubble lift coefficient C_L is different, the bubble lift will point to the center of the channel or the wall, so that the radial distribution of the bubble share corresponds to the parabolic distribution of the center height or the saddle distribution of the wall peak. In addition, the value of the lift coefficient C_L will significantly affect the radial distribution of void fraction gradient. The main models of lift coefficient are summarized in Table **3**.

Table 2: Mathematical expressions of drag force coefficients.

References	Mathematical Expressions
Grace [8] (1976)	$C_D = max\left(C_D(sphere), min\left(C_D(ellipse), C_D(cap)\right)\right)$ $C_D(sphere) = \begin{cases} \frac{24}{Re_b} & Re_b \le 0.01 \\ max\left(\frac{24}{Re_b}(1+0.15Re_b^{0.687}), 0.44\right) & 0.01 < Re_b \end{cases}$ $C_D(cap) = \frac{8}{3}$ $C_D(ellipse) = \frac{4}{3}\frac{gd_b}{U_t^2}\frac{(\rho_l - \rho_g)}{\rho_l}$ $U_t = \frac{\mu_l}{\rho_l d_b} Mo^{-0.149}(J - 0.857)$ $J = \begin{cases} 0.94H^{0.757} & 2 < H \le 59.3 \\ 3.42H^{0.441} & H > 59.3 \end{cases}$ $H = \frac{4}{3} EoMo^{-0.149}\left(\frac{\mu_l}{9\times 10^{-4}}\right)^{-0.14}$
Ishii and Zuber [20] (1979)	$C_D = max\left(C_D(sphere), min\left(C_D(ellipse), C_D(cap)\right)\right)$ $C_D(sphere) = \begin{cases} \frac{24}{Re_b} & Re_b \le 0.01 \\ max\left(\frac{24}{Re_b}(1+0.15Re_b^{0.687}), 0.44\right) & 0.01 < Re_b \end{cases}$ $C_D(cap) = \frac{8}{3}$ $C_D(ellipse) = \frac{2}{3} Eo^{1/2}$
Tomiyama [21] (1998)	$C_D = max\left(min\left(\frac{24}{Re_b}(1+0.15Re_b^{0.687}), \frac{72}{Re_b}\right), \frac{8}{3}\frac{Eo}{Eo+4}\right)$
Simonnet *et al*. [22] (2007)	$C_D = C_{D\infty} E_\infty$ $C_{D\infty} = \frac{4}{3}\frac{\rho_l - \rho_g}{\rho_l}\frac{gd_b}{U_t^2}$ $U_t = \frac{u_{b1}u_{b2}}{\sqrt{u_{b1}^2 + u_{b2}^2}}$ $u_{b1} = \frac{1}{18}\frac{\rho_l - \rho_g}{\mu_l} g d_b^2 \left(\frac{3\mu_g + 3\mu_l}{3\mu_g + 2\mu_l}\right)$ $u_{b2} = \sqrt{\frac{2\sigma}{d_b(\rho_l - \rho_g)} + \frac{gd_b}{2}}$ $E_\infty = (1-\alpha_g)\left[(1-\alpha_g)^m + \left(4.8\frac{\alpha_g}{1-\alpha_g}\right)^m\right]^{-2/m}, m = 25$

2.3.3. Wall Lubrication Force

When the bubble is close to the wall, if the diameter of the bubble is small enough to deform and can remain spherical or nearly spherical, then the velocity of the liquid fluid between the bubble and the wall further decreases, and the pressure on the side of the bubble near the wall increases. The force on the bubble pointing to the center of the flow channel is called wall lubrication force. The formula of wall lubrication force per unit volume is as follows:

$$\vec{F}_g^{\,WL} = -C_{WL}\rho_l\alpha_g\left\|\vec{U}_g - \vec{U}_l\right\|^2\vec{n}_w \tag{10}$$

where C_{WL} is wall lubrication force coefficient and $\vec{n}_w$ is the unit normal vector pointing to the outside of the tube, so the force direction points to the inside of the tube, preventing the bubble from contacting the wall.

Table 3: Mathematical expressions of the coefficients of lift force.

References	Mathematical Expressions
Saffman [23] (1965), Mei and Klausner [24] (1994)	$C_L = \frac{3}{2\pi\sqrt{Re_\omega}} C_L'$ $C_L' = \begin{cases} 6.46 f(Re_b, Re_\omega) & Re_b < 40 \\ 6.46 * 0.0524(\beta Re_b)^{1/2} & 40 < Re_b < 100 \end{cases}$ $\beta = \frac{1}{2}\frac{Re_\omega}{Re_b}$ $f(Re_b, Re_\omega) = (1 - 0.3314\beta^{1/2}) e^{-0.1 Re_b} + 0.3314\beta^{1/2}$
Legendre and Magnaudet [25] (1998)	$C_L = \sqrt{\left(C_{L,low\ Re}\right)^2 + \left(C_{L,high\ Re}\right)^2}$ $C_{L,low\ Re} = \frac{6}{\pi^2}(Re_b Sr)^{-1/2} J'(\varepsilon)$ $C_{L,high\ Re} = \frac{1}{2}\frac{1 + 16Re_b^{-1}}{1 + 29Re_b^{-1}}$ $\varepsilon = \sqrt{\frac{2\beta}{Re_b}}$ $J(\infty) = 2.55$ $0.1 \le Re_b \le 500, Re_\omega \le Re_b$
Tomiyama [21] (1998)	$C_L = \begin{cases} min[0.288 tanh(0.121 Re_b), f(Eo_H)] & Eo_H \le 4 \\ f(Eo_H) & 4 < Eo_H \le 10 \\ -0.27 & 10 < Eo_H \end{cases}$ $f(Eo_H) = 0.00105 Eo_H^3 - 0.0159 Eo_H^2 - 0.0204 Eo_H + 0.474$ $Eo_H = \frac{g(\rho_l - \rho_g) d_H^2}{\sigma}$ $d_H = d_b (1 + 0.163 Eo^{0.757})^{1/3}$

Table **4** summarizes the main models of wall lubrication force coefficient C_{WL}.

Table 4: Mathematical expressions of the coefficients of wall lubrication force.

References	Mathematical Expressions
Antal *et al*. [9] (1991)	$C_{WL} = max\left\{0, \frac{C_{W1}}{d_b} + \frac{C_{W2}}{y_w}\right\}$ $C_{W1} = -0.01, C_{W2} = 0.05$
Tomiyama [21] (1998)	$C_{WL} = C_W(Eo)\frac{d_b}{2}\left(\frac{1}{y_w^2} - \frac{1}{(D - y_w)^2}\right)$ $C_W(Eo) = \begin{cases} 0.47 & Eo < 1 \\ e^{-0.933 Eo + 0.179} & 1 \le Eo \le 5 \\ 0.00599 Eo - 0.0187 & 5 < Eo \le 33 \\ 0.179 & 33 < Eo \end{cases}$
Hosokawa *et al*. [14] (2002)	$C_{WL} = C_W(Re_b, Eo)\frac{2}{d_b}\left(\frac{d_b}{2y_w}\right)^2$ $C_W(Re_b, Eo) = max\left(\frac{7}{Re_b^{1.9}}, 0.0217 Eo\right)$
Frank [26] (2008)	$C_{WL} = C_W(Eo) \cdot max\left\{0, \frac{1}{C_{WD}} \cdot \frac{1 - \frac{y_w}{C_{WC} d_b}}{y_w \cdot \left(\frac{y_w}{C_{WC} d_b}\right)^{p^* - 1}}\right\}$ $C_{WC} = 10, C_{WD} = 6.8, p^* = 1.7$ $C_W(Eo) = \begin{cases} 0.47 & Eo < 1 \\ e^{-0.933 Eo + 0.179} & 1 \le Eo \le 5 \\ 0.00599 Eo - 0.0187 & 5 < Eo \le 33 \\ 0.179 & 33 < Eo \end{cases}$

2.3.4. Turbulent Dispersion Force

Due to the interaction between the discrete phase and the turbulent vortex around it, phase diffusion occurs when there is a large volume fraction gradient in the flow field due to the turbulence of the continuous phase. The bubble will move to the sidewall under the influence of turbulence so that the radial distribution of gas holdup tends to be uniform. Lopez de Bertodano [27] puts forward the model expression of turbulent dispersion force, as shown below:

$$\vec{F}_g^{\,TD} = -C_{TD}\rho_l k_l \nabla\alpha_g \tag{11}$$

However, there is no universal expression of turbulent dispersion force coefficient C_{TD} at present. For bubble flow, C_{TD} is generally between 0.1 and 1.0. Burns *et al*. [28] developed the FAD model in 2004, in which the turbulent dispersion force is modeled based on the time average of the interphase drag term and expressed in the form of the Favre average. The formula of the FAD model is as follows:

$$\vec{F}_{TD} = -C_{TD}C_{cd}\frac{\mu_{tl}}{\rho_l\sigma_{tl}}\left(\frac{\nabla\alpha_g}{\alpha_g} - \frac{\nabla\alpha_l}{\alpha_l}\right) \tag{12}$$

where, $C_{cd} = \frac{3}{4}\frac{C_D}{d_b}\alpha_g\rho_l\left|\vec{U}_g - \vec{U}_l\right|, C_{TD} = 1.0, \sigma_{tl} = 0.9$.

In general, since the coefficient of Lopez de Bertodano is uncertain, it is best to use the FAD model.

2.3.5. Virtual Mass Force

A virtual mass force will be generated when there is a relative acceleration between the two phases. This force is especially important for accelerated flow (rotation of bubbles) or when the density of the continuous phase is much greater than that of the discrete phase. The expression is:

$$F_{VM} = C_{VM}\rho_l\alpha_g\frac{D}{Dt}(\overline{U}_g - \overline{U}_l) \tag{13}$$

where C_{VM} is the virtual mass force coefficient,a_k is the acceleration of k phase.

Some researchers believe that the role of virtual mass force in gas-liquid boiling flow is limited, so the influence of virtual mass force is not introduced into the calculation. On the other hand, because the virtual mass force is used in the mainstream flow direction, it does not affect the radial distribution of the bubble share, so it is not considered in many CFD calculations which focus on the radial distribution of bubbles.

3. Research Object and Numerical Method

The research object in the present study is the DEDALE experiment carried out by French Electric Power Company EDF [19]. In 1995, EDF carried out DEDALE experiments to study the axial development of adiabatic air-blister flow in vertical pipes. The test section of the DEDALE experiment is a pipe with an inner diameter of 38.1mm and a height of 6m. The experiment is conducted under ambient pressure and temperature, and the local parameters at different axial positions are measured. The DEDALE experiment includes several groups of working conditions under different air and water mass flow combinations. In this paper, a group of experimental DEDALE1101 is selected to simulate, and the inlet conditions of the experiment are shown in Table **5**.

Table 5: DEDALE1101 experimental inlet conditions.

Parameters	Values
J_l	0.877m/s
J_g	0.0588m/s
α_g	0.048
k_l	$4.23\times10^{-3}m^2/s^2$
a_i	$97m^{-1}$

All inlet parameters, such as liquid and gas mass flow and vacuole share, are evenly distributed. At the outlet, atmospheric pressure is used as a boundary condition. The liquid phase is set to a no-slip boundary condition on the wall surface, and the gas phase is set to a free-slip boundary condition. Based on the results of some previous studies, the gas phase is assumed to be laminar flow, and the turbulence in the liquid phase is described by the enhanced k-ε model of Sato *et al*. [29]. In this work, because the order of magnitude of the characteristic void fraction in the DEDALE experiment is too small, the phenomenon of bubble breakage and coalescence is very weak and can be ignored. Therefore, the constant bubble diameter assumption adopted in this study means that the dispersed phase is assumed to be a monodisperse spherical bubble group, but it is a polydisperse bubble group. For the following analysis, the average bubble Reynolds number Re_b needs to be estimated by the following formula:

$$U_{sl} = \sqrt{\frac{4(\rho_l - \rho_g)d_b g}{3C_D\rho_l}} \tag{14}$$

For all cases, Re_b ranges from 700 to 2000. The two-fluid solver in OpenFOAM is employed to calculate the two-phase flow of the DEDALE experiment. The solver uses the finite volume method and high-resolution discretization scheme. The QUICK scheme discretizes the volume fraction, and the remaining convection terms are discretized by the second-order upwind scheme. The PIMPLE algorithm is used to couple pressure and velocity. For all simulations, as the simulations carried out in this study have been developed in the framework of the steady flow hypothesis, the evoked time step seems to be a numerical variable used in solving process. The initial time step is set to 0.001 seconds, the number of iterations per time step is set to a fixed value of 40, and the rms residual of 1×10^{-4} is selected as the convergence criterion.

A schematic diagram of the geometry of the numerical simulation is shown in Figure **3**: The two-phase flow of the fully developed segment of the tube is bubbly. The gas-phase of the bubbly flow is dispersed, and the liquid phase is continuous. In the experiment, the tube diameter is 38.1mm, and the bubbles have a large gap in the channel. The shape of the bubbles is spherical, and the bubbles in the bubbly flow are separated from each other and dispersed in the liquid phase.

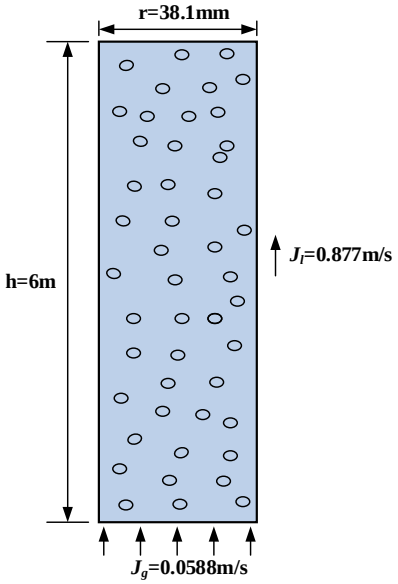

Figure 1: Schematic diagram of the geometry.

The solver in OpenFOAM will also generate three-dimensional geometry to solve two-dimensional problems. When solving two-dimensional problems, there is no need to mesh in the direction where the equation is not solved, and wedge boundary conditions are used at the corresponding boundary. Because the structure of the DEDALE experimental section is simple and the two-phase flow parameters in the circular pipe will hardly change in the circumferential direction of the pipe, the wedge geometry parallel to the centerline of the circular pipe is

adopted in the calculation. As shown in the centerline of the circular tube is parallel to the height of the wedge geometry. The wedge boundary type is used, and the actual calculation domain is the triangular prism in the figure below. In this way, it can effectively reduce the amount of calculation and improve calculation efficiency.

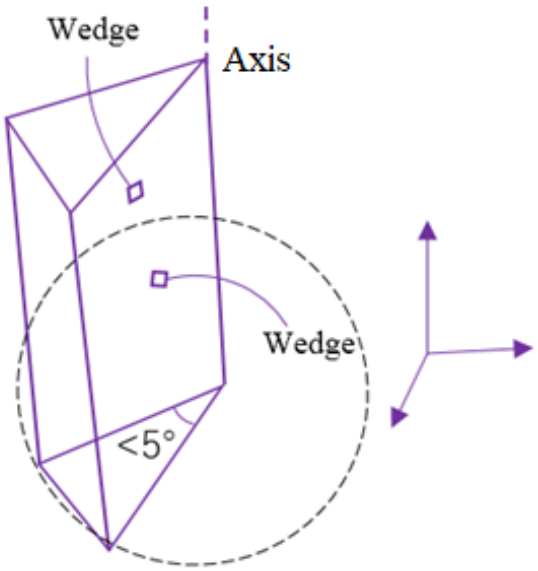

Figure 2: Axisymmetric geometry.

Five meshes with different mesh numbers are used for mesh independence verification. The mesh independence verification was carried out using the Ishii-Zuber drag force model, the Tomiyama lift model, the Antal wall lubrication force model, and the Lopez de Bertodano turbulent dispersion force model. The virtual mass force coefficient was set to 0.5. Figure **3**: compares the calculation results under different meshes. As shown in the figure, when the number of meshes is increased to 10000, it shows good independence. Therefore, the number of meshes is divided into 10000 in the later calculations.

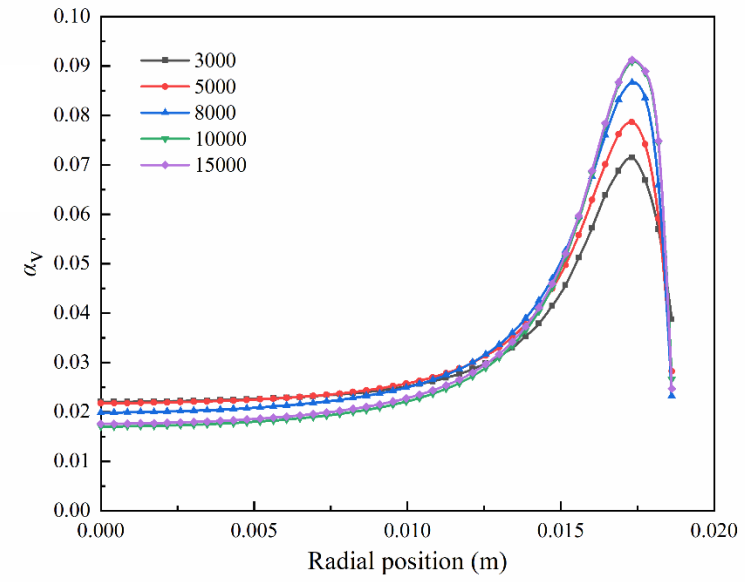

Figure 3: Mesh independence verification.

Figure **4:** Mesh of the DEDALE experimental section shows the wedge-shaped grid used in the air-water two-phase flow experiment. It is divided into 100 grids in the axial direction and 100 grids in the radial direction. The grid expansion rate is (0.1, 0.1, 1.0).

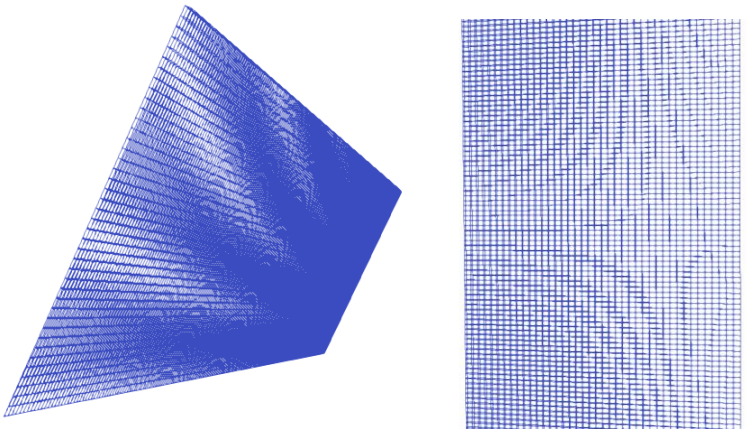

Figure 4: Mesh of the DEDALE experimental section.

In order to obtain the two-phase flow state of the fully developed stage, the local parameters near the outlet (y/D=155) were obtained and compared with the corresponding experimental data.

4. Results and Discussions

4.1. Combination of Interphase Force Models

So far, domestic and foreign scholars have done much research on the interphase force and put forward a variety of models for each interphase force. However, most of these models are studied independently, and the models of single or several interphase forces are considered, respectively. There is no comprehensive comparison of the effects of different model combinations of drag force, lift force, turbulent dispersion force, wall lubrication force, and virtual mass force on two-phase flow.

In order to obtain the numerical simulation performance under different interphase force model combinations, this study selects part of the interphase force model to combine, and combined with the interphase force model combination proposed by some scholars. As shown in Table **6**, nine interphase force model combinations are obtained. The DEDALE1101 experiment is simulated and compared with the experimental values of local parameters.

Table 6: Interphase force model combination.

Model	References	Drag Force	Lift Force	Turbulent Dispersion Force	Wall Lubrication Force	Virtual Mass Force
model1	Chen *et al.* [30] (2019)	Ishii-Zuber	Moraga	Lopez de Bertodano	–	–
model2	Wang and Sun [31] (2010)	Tomiyama	Tomiyama	0.1	Antal	–
model3	Jin *et al.* [32] (2019)	Tomiyama	Legendre and Magnaudet	–	Frank	–
model4	Parekh and Rzehak [33] (2018)	Ishii-Zuber	Tomiyama	FAD	–	0.5
model5	Mohd Akbar *et al.* [34] (2013)	Tomiyama	Tomiyama	Lopez de Bertodano	–	0.5
model6	Rzehak and Krepper [35] (2013)	Tomiyama	Tomiyama	FAD	Antal	–
model7	Marfaing *et al.* [36] (2018)	Ishii-Zuber	Tomiyama	Burns	Tomiyama	–
model8	–	Ishii-Zuber	Tomiyama	Gosman	Tomiyama	–
model9	–	Ishii-Zuber	Tomiyama	Lopez de Bertodano	Antal	0.5

4.2. Calculation Results

In the calculation, the bubble diameter is about 3 mm, the same as the inlet. The calculated void fraction, gas velocity, and liquid velocity are shown in Figure **5-7**, respectively. In the figure, the abscissa origin represents the central position of the pipe, and the other coordinates represent the distance from the center of the pipe. The longitudinal axis refers to the ratio between the calculated result and the experimental value. It can be seen from that near the wall, the calculated value of the void fraction of each model is different from the experimental value, and the simulated "near wall" peak has an enhancement or inhibition effect. In general, the radial distribution of the void fraction obtained by model 7 agrees with the experimental data, and the phase distribution of the center of the channel is well predicted in the simulation.

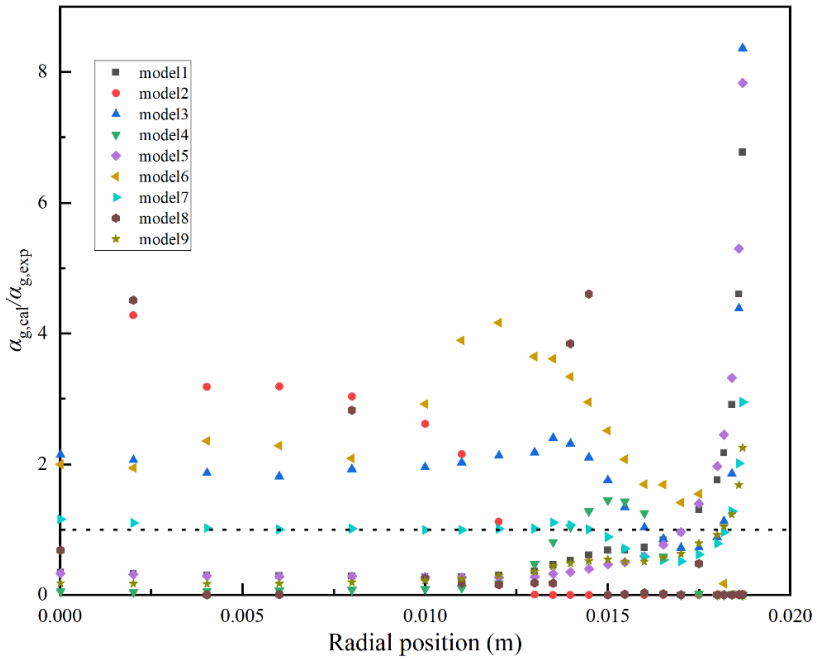

Figure 5: The radial distribution of the void fraction.

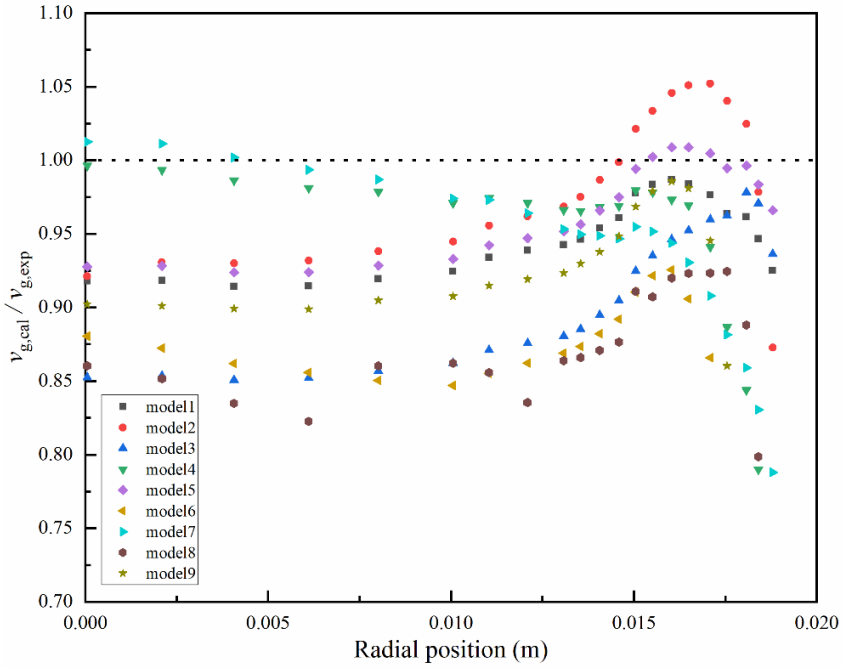

Figure 6: Radial distribution of gas velocity.

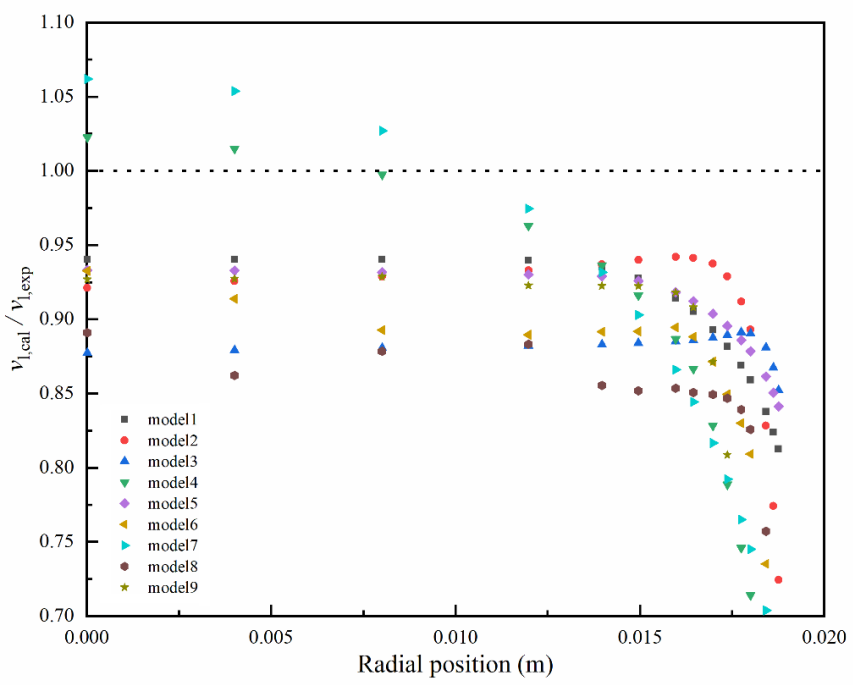

Figure 7: Radial distribution of liquid velocity.

As can be seen from Figure **6** and Figure **7**, for gas velocity and liquid velocity, the calculated values of each model combination are slightly lower than the experimental values, and the errors between the calculated values and the experimental values near the center of the channel are basically within ±15%. There is only a large error near the wall. The predicted values obtained by model4 and model7 are closest to the experimental values.

4.3. Results Analysis

In order to quantitatively analyze the numerical performance of each interphase force model combination and evaluate the accuracy of the calculation results of each model combination, the maximum error E_m and root mean square error $\bar{E}$ between the numerical results of each interphase force model combination and the corresponding experimental value are calculated. E_m and $\bar{E}$ are calculated by the following formula:

$$E_m = max\left|\frac{x_{i,cal} - x_{i,exp}}{x_{i,exp}}\right| \tag{3}$$

$$\bar{E} = \sqrt{\frac{1}{m}\sum_{i=1}^{m}\left(x_{i,cal} - x_{i,exp}\right)^2} \tag{4}$$

E_m and $\bar{E}$ in different cases are shown in Table **7**. It can be seen from Table **7** that among the nine groups of models established, the errors between the simulation results of model 7 and the experimental data in terms of void fraction, gas velocity, and liquid velocity are the smallest. In other words, the combination of Ishii-Zuber drag model, Tomiyama lift model, Burns turbulent dispersion force model, and Tomiyama wall lubrication force model has the best performance under the present bubbly flow conditions.

5. Conclusions and Outlook

In this study, the bubbly flow in a vertical tube is simulated, and the interphase force model combinations, including drag force, lift force, wall lubrication force, turbulent dispersion force, and virtual mass force, are adopted. The effects of interphase forces on the distribution of local parameters such as void fraction, gas velocity, and liquid velocity are analyzed. The maximum error and root mean square error between the calculated and

experimental values of each model combination are calculated. A set of optimal model combinations is obtained through the quantitative comparison of each model.

Table 7: The error between the calculated value and the experimental value of each model combination.

Model	Void Fraction		Gas Velocity (m/s)		Liquid Velocity (m/s)	
	E_m	$\overline{E}$	E_m	$\overline{E}$	E_m	$\overline{E}$
M1	0.12205	0.04904	0.10965	0.07210	0.19061	0.12326
M2	0.34438	0.09981	0.14215	0.06478	0.20511	0.12023
M3	0.15575	0.05339	0.19085	0.13063	0.25171	0.15518
M4	0.10694	0.04591	0.33965	0.10652	0.26362	0.18279
M5	0.14455	0.05895	0.09735	0.05855	0.19811	0.12317
M6	0.13663	0.07560	0.72777	0.29746	0.23142	0.16909
M7	0.05184	0.02188	0.23665	0.09346	0.19542	0.15559
M8	0.16806	0.07398	0.52845	0.19546	0.26881	0.18528
M9	0.04301	0.02894	0.78935	0.23949	0.66612	0.32158

Under the present bubbly flow conditions, the interphase force model combination of the Ishii-Zuber drag model, Tomiyama lift model, Tomiyama wall lubrication force model, and Burns turbulent dispersion force model can give better simulation results. It should be noted that the combination of models obtained in this study is limited to a certain range of flow conditions, so more simulations should be carried out in order to extend the optimal combination of interphase force models to more extensive working conditions in the future.

Acknowledgments

The authors are grateful for the support of the National Natural Science Foundation of China (No. U1867219; No. 51806023).

References

[1] Tomiyama A. Struggle With Computational Bubble Dynamics[J]. Multiphase Science Technology,1998, 10(4): 369-405. https://doi.org/10.1615/MultScienTechn.v10.i4.40

[2] Lucas D, Krepper E, Prasser H M. Use of models for lift, wall and turbulent dispersion forces acting on bubbles for poly-disperse flows[J].Chemical Engineering Science,2007, 62(15): 4146-4157. https://doi.org/10.1016/j.ces.2007.04.035

[3] Lucas D, Krepper E, Prasser HM. Development of co-current air-water flow in a vertical pipe[J]. International Journal of Multiphase Flow,2005, 31(12): 1304-1328. https://doi.org/10.1016/j.ijmultiphaseflow.2005.07.004

[4] Horst-Michael, Prasser, And, *et al*. Evolution of the structure of a gas-liquid two-phase flow in a large vertical pipe[J]. Nuclear Engineering Design,2007, 237: 1848-1861. https://doi.org/10.1016/j.nucengdes.2007.02.018

[5] Burns A D, Frank, T, Hamill, I, Shi, J.-M. The Favre averaged model for turbulence dispersion in Eulerian multi-phase flows[C].5 Th Int Conf Multiphase Flow, Icmf,2004: ICMF 1-17.

[6] Yamoah S, Martínez-Cuenca, R, Monrós, G, Chiva, S, Macián-Juan, R.Numerical investigation of models for drag, lift, wall lubrication and turbulent dispersion forces for the simulation of gas-liquid two-phase flow[J]. Chemical Engineering Research and Design,2015, 98: 17-35. https://doi.org/10.1016/j.cherd.2015.04.007

[7] Monrós-Andreu G, Chiva S, Martínez-Cuenca R, *et al*.Water temperature effect on upward air-water flow in a vertical pipe: Local measurements database using four-sensor conductivity probes and LDA[J].2013. https://doi.org/10.1051/epjconf/20134501105

[8] Grace J, Th N. Shapes and velocities of single drops and bubbles moving freely through immiscible liquids[J]. Chemical Engineering Research and Design,1976, 54: 167-173.

[9] Antal SP, Jr R, Flaherty JE. Analysis of phase distribution in fully developed laminar bubbly two-phase flow[J].1991, 17(5): 635-652. https://doi.org/10.1016/0301-9322(91)90029-3

[10] Wang Q, Wei Y J I J O H, Transfer M. Computation and validation of the interphase force models for bubbly flow[J].2016, 98: 799-813. https://doi.org/10.1016/j.ijheatmasstransfer.2016.03.064

[11] Hibiki T, Ishii M, Xiao Z J I J O H, *et al*. Axial interfacial area transport of vertical bubbly flows[J].2001, 44(10): 1869-1888. https://doi.org/10.1016/S0017-9310(00)00232-5

[12] Fu X. Interfacial area measurement and transport modeling in air-water two-phase flow[D]. Purdue University,2001.

[13] Ishii M, Zuber N.Drag coefficient and relative velocity in bubbly, droplet or particulate flows[J].AIChE Journal,1979, 25(5): 843-855. https://doi.org/10.1002/aic.690250513

[14] Hosokawa S, Tomiyama A, Misaki S, *et al*. Lateral migration of single bubbles due to the presence of wall[C].Fluids Engineering Division Summer Meeting,2002: 855-860. https://doi.org/10.1115/FEDSM2002-31148

[15] Saffman P G J J O F M.The Lift on a Small Sphere in a Slow Shear[J].1965, 22(2): 385-400. https://doi.org/10.1017/S0022112065000824

[16] Mei R, Klausner J F J I J O H, Flow F. Shear lift force on spherical bubbles[J].1994, 15(1): 62-65. https://doi.org/10.1016/0142-727X(94)90031-0

[17] Moraga F J, Bonetto FJ, Lahey R T J I J O M F. Lateral forces on spheres in turbulent uniform shear flow[J].1999, 25(6-7): 1321-1372. https://doi.org/10.1016/S0301-9322(99)00045-2

[18] Liao Y, Ma T, Liu L, *et al*.Eulerian modelling of turbulent bubbly flow based on a baseline closure concept[J].2018, 337(OCT.): 450-459. https://doi.org/10.1016/j.nucengdes.2018.07.021

[19] Michta E. Modeling of subcooled nucleate boiling with OpenFOAM[J]. 2011.

[20] Ishii, M. and Zuber, N. Drag coefficient and relative velocity in bubbly, droplet or particulate flows[J].1987, 25: 843-855. https://doi.org/10.1002/aic.690250513

[21] Tomiyama A. Struggle With Computational Bubble Dynamics[J]. Multiphase Science and Technology, 1998, 10(4):369-405. https://doi.org/10.1615/MultScienTechn.v10.i4.40

[22] Simonnet M, Gentric C, Olmos E, *et al*. Experimental determination of the drag coefficient in a swarm of bubbles[J]. Chemical Engineering Science, 2007, 62(3):858-866. https://doi.org/10.1016/j.ces.2006.10.012

[23] Saffman PG. The Lift on a Small Sphere in a Slow Shear[J]. Journal of Fluid Mechanics, 1965, 22(2):385-400. https://doi.org/10.1017/S0022112065000824

[24] Mei R, Klausner J F. Shear lift force on spherical bubbles[J]. International Journal of Heat and Fluid Flow, 1994, 15(1):62-65. https://doi.org/10.1016/0142-727X(94)90031-0

[25] Legendre D, Magnaudet J. The lift force on a spherical bubble in a viscous linear shear flow[J]. Journal of Fluid Mechanics, 1998, 368:81-126. https://doi.org/10.1017/S0022112098001621

[26] Frank T, Zwart P J, Krepper E, *et al*. Validation of CFD models for mono- and polydisperse air-water two-phase flows in pipes[J]. Nuclear Engineering & Design, 2008, 238(3):647-659. https://doi.org/10.1016/j.nucengdes.2007.02.056

[27] Bertodano M, Lahey R T, Jones O C. Turbulent bubbly two-phase flow data in a triangular duct[J]. Nuclear Engineering and Design, 1994, 146(1-3):43-52. https://doi.org/10.1016/0029-5493(94)90319-0

[28] Burns A D, Frank T, Hamill I, *et al*. The Favre averaged drag model for turbulent dispersion in Eulerian multi-phase flows[C]// 5th International Conference on Multiphase Flow, ICMF'04. 2004.

[29] Sekoguchi Y S. Liquid velocity distribution in two-phase bubble flow[J]. International Journal of Multiphase Flow, 1975.

[30] Chen Q, Podila K, Rao Y F, *et al*. Assessment of CFD for unheated gas-liquid flows with high void fraction[J]. Nuclear Engineering and Design, 2018, 341(JAN.):346-359. https://doi.org/10.1016/j.nucengdes.2018.11.016

[31] Xia W, Sun X. Three-dimensional simulations of air-water bubbly flows[J]. Int.j.multiphase Flow, 2010, 36(11-12):882-890. https://doi.org/10.1016/j.ijmultiphaseflow.2010.08.004

[32] Jin D, Xiong J, X Cheng. Investigation on interphase force modeling for vertical and inclined upward adiabatic bubbly flow[J]. Nuclear Engineering and Design, 2019, 350(AUG.):43-57. https://doi.org/10.1016/j.nucengdes.2019.05.005

[33] Parekh J, Rzehak R. Euler-Euler multiphase CFD-simulation with full Reynolds stress model and anisotropic bubble-induced turbulence[J]. International Journal of Multiphase Flow, 2017:S0301932217304275. https://doi.org/10.1016/j.ijmultiphaseflow.2017.10.012

[34] Akbar M, Hayashi K, Lucas D, *et al*. Effects of inlet condition on flow structure of bubbly flow in a rectangular column[J]. Chemical Engineering Science, 2013, 104(50):166-176. https://doi.org/10.1016/j.ces.2013.09.019

[35] Rzehak R, Krepper E. CFD modeling of bubble-induced turbulence[J]. International Journal of Multiphase Flow, 2013, 55(Complete):138-155. https://doi.org/10.1016/j.ijmultiphaseflow.2013.04.007

[36] A O M, B M G, J. Laviéville b, *et al*. Comparison and uncertainty quantification of two-fluid models for bubbly flows with NEPTUNE_CFD and STAR-CCM+[J]. Nuclear Engineering and Design, 2018, 337:1-16. https://doi.org/10.1016/j.nucengdes.2018.05.028